A LETTERS JOURNAL EXPLORING THE FRONTIERS OF PHYSICS

LETTER

Focusing of liquid surface waves by gradient index lens

To cite this article: Zhenyu Wang *et al* 2014 *EPL* **108** 24003

A Letters Journal Exploring the Frontiers of Physics

October 2014

EPL, **108** (2014) 24003 www.epljournal.org
doi: 10.1209/0295-5075/108/24003

Focusing of liquid surface waves by gradient index lens

Zhenyu Wang[(a)], Pei Zhang, Xiaofei Nie and Yongqiang Zhang

College of Civil Engineering and Architecture, Zhejiang University - Hangzhou 310058, PRC

received 16 August 2014; accepted in final form 1 October 2014
published online 20 October 2014

PACS 47.35.-i – Hydrodynamic waves
PACS 47.90.+a – Other topics in fluid dynamics
PACS 92.05.Jn – Ocean energy extraction

Abstract – In the long-wavelength limit, a periodic array of bottom-mounted vertical cylinders may be used as a homogeneous medium for liquid surface waves and their effective parameters, such as their refractive index, depending on the filling fraction of the cylinders. Based on this effective medium theory, a gradient index (GRIN) lens for the focusing of liquid surface waves has been designed and fabricated here through the gradual modification of the cylinder filling fraction along a direction perpendicular to the lens axis. Their focusing performance and the transmission properties for liquid surface waves are then studied both experimentally and numerically. Both the wave patterns and spatial intensities obtained by experiment and numerical calculation demonstrate that the GRIN lens is able to focus planar liquid surface waves within a certain frequency region.

Introduction. – There is currently an increasing amount of interest being shown in hydroelectric power and tidal power, owing to the fact that they are clean energies. Increasing the harvest efficiency of water or ocean waves is one of the key problems to be found in the utilization of these sources of power. Hence, the manipulation of liquid surface waves —focusing and collimation of waves, for example— is needed and can be used for the concentration of wave energy.

Liquid surface waves represent an important kind of classic wave with similar characteristics to other kinds —electromagnetic and sound waves, for example. In recent years, rapid strides have been made in terms of scientific research concerning the propagation of electromagnetic (sound) waves in photonic (phononic) crystals [1–21]. Their novel properties contribute to many interesting phenomena in wave propagation and new approaches to wave control, such as superlensing [9,10], double negative nature [11,12], cloaking [13,14], and directional emission [15–21]. As with electromagnetic and sound waves, liquid surface waves are also modulated by multiple Bragg scatterings when propagating in periodic structures. Previous research has verified that the propagation of liquid surface waves in periodic structures is also characterized by band structures and band gaps [22–29]. In previous research, many characteristics similar to those realized by using photonic and phononic crystals, including lensing effects [30–32], wave focusing [33,34], self-collimation [35], negative effective gravity [36,37], directional emission [38–40], cloaking [41], and wave rotation [42], have been demonstrated with respect to liquid surface waves. Similar interesting phenomena in relation to photonic and phononic crystals can thus be observed visually in experiments involving liquid surface waves. More importantly, many new approaches to controlling the waves in rivers and oceans could potentially be realized based on their own unique properties.

Since liquid surface waves also follow the Bloch theorem when they propagate through periodic structures, the effective medium theory utilized for photonic and phononic crystals can also be extended to the research of liquid surface waves. It is known that in the long-wavelength limit, phononic crystals behave like homogeneous media whose effective acoustic parameters basically depend on the lattice filling fraction [43]. In 2005, Hu and Chan demonstrated theoretically that, in the long-wavelength limit, water waves propagated through an array of bottom-mounted vertical cylinders as if water had an effective depth and effective gravitational constant and there was an effective refractive index which could be used with the Snell refractive law [33]. Based on this feature, they further proposed a water wave lens consisting of a biconvex array of bottom-mounted vertical cylinders, similar

(a) E-mail: wzyu@zju.edu.cn (corresponding author)

to that used for sonic waves. Afterwards, their idea was experimentally verified for liquid surface waves by Yang *et al.* [34]. Their research provided a mechanism for controlling liquid surface waves so that it would be possible to enhance the utilization of ocean wave energy through periodic structures.

The focusing properties of the lenses studied above are based on their external curved surfaces. The gradient index (GRIN) lens, however, is another type of focusing lens that has been fabricated for the focusing of light and acoustic waves [44–48]. A GRIN lens, which is achieved by the gradual modification of a lattice filling fraction, has a flat surface and is easier to fabricate than a curved lens. However, to date, there has been no research concerning the application of a GRIN lens for liquid surface waves. As a result, it is the focusing of liquid surface waves by applying a GRIN lens that is under investigation in this paper.

Theory and experiment. – A GRIN is often used to describe an inhomogeneous medium in which the refractive index varies from point to point. As shown in fig. 1(a), if the index profile varies continuously from the x-axis to the edges along the y-axis, the medium can curve the waves which propagate through it along the x-axis direction so as to focus them at a given point. Like the GRIN sonic lenses designed for sound focusing [47,48], the refractive index of a GRIN lens for liquid surface waves can be given by the formula

$$n(y) = n_0 \operatorname{sech}(\alpha y), \tag{1}$$

where α is a constant defined as

$$\alpha = \frac{1}{h}\cosh^{-1}\left(\frac{n_0}{n_h}\right), \tag{2}$$

where h is the half-height of the lens, n_0 is the refractive index on the x-axis ($y = 0$) and n_h is the refractive index at the lens edges ($y = \pm h$). This refractive index profile in the form of a hyperbolic secant ensures that the wave focusing property can be realized with minimum aberration.

In order to realize the GRIN medium for liquid surface waves, there is a method to change the wave depth by using the uneven bottom with gradient height, which is then based on the similarity between the shallow water surface wave equation and the electromagnetic equation [42]. Another technique utilizes periodic structures to construct equivalent refractive indexes. For instance, various effective refraction indexes can be realized by using a periodic array of cylinders at the different wavelengths of waves and filling fractions of cylinders.

When liquid surface waves propagate through an array of vertical cylinders, their dispersion relation $k(\mathbf{Q})$, where $\mathbf{Q}$ is the Bloch wave vector, can be accurately calculated by using the multiple scattering method. Since the dispersions are approximately isotropic and linear when

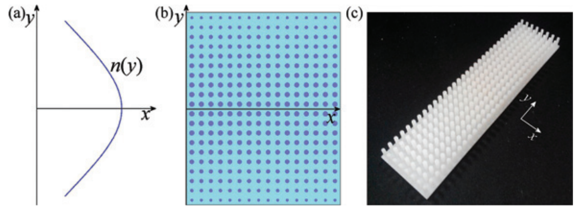

Fig. 1: (Color online) (a) The distribution of the refractive index of a GRIN lens. (b) A GRIN lens that is realized by adjusting the radii of cylinders along the y-axis to achieve a hyperbolic secant refractive index profile. (c) Experimental sample of the GRIN lens for liquid surface waves.

$ka < 0.5\pi$, namely, $\lambda > 4a$, where k is the wave number, a is the lattice constant, and λ is the wavelength, the effective index can be defined as $n_{eff} = |\mathbf{Q}|/k$. In addition, it is also found from dispersion calculations that n_{eff} merely depends on and increases with the increased cylinder filling fraction. Accordingly, a GRIN lens for liquid surface waves of long wavelength can be designed and fabricated by a gradual modification of the cylinder filling fraction along the direction perpendicular to the x-axis, as is shown in fig. 1(b).

In this study, the GRIN lens constructed by using cylinder arrays has been designed with a profile $n(y)$ according to eq. (1) with $n_0 = 1.15$ and $n_h = 1.075$. The vertical rigid cylinders were distributed in a square lattice with the lattice parameter $a = 5$ mm. Figure 1(c) shows the photo of the sample GRIN lens in the experiment. The radius r_l of the cylinder in the l layer was obtained by a reverse calculation from dispersion relations, where subscript l represents the layer's number along the $+y$-direction. The values of r_l obtained are shown in table 1. It should be noted that only values corresponding to the upper half of the GRIN lens have been provided, since the lens is symmetrical with respect to the x-axis.

The experiment has been carried out in a horizontally placed vessel consisting of a rectangular glass bottom and four 10° slope wave-absorbing sides. To accord with other research [29,30,34,35,42], a special liquid with a very small capillary length (1.09 mm) was used to minimize the capillary effects. The GRIN lens, which was fabricated by a 3D printer to achieve high precision, was placed on the bottom of the vessel. The lens consisted of eight rows of cylinder arrays with a height of 10 mm, and the cylinders were fixed on a thin plate in order to maintain the correct arrangement. The liquid depth was $H = 5$ mm over the plexiglass plate. At the top of the vessel, a glass lid was placed to prevent the evaporation of the liquid. A LED lamp was hung 1.2 m above the vessel. The light passing through the vessel was reflected onto the screen by placing a mirror below it so that the projected images of liquid surface wave patterns could be visualized and then captured using a digital camera. A plane-wave generator was placed about 6 cm away from the cylinder array and its amplitude and frequency tuned precisely by using a

Table 1: Radius profile $r_l(y)$ of the cylinders in the GRIN lens fabricated here.

l	1	2	3	4	5	6	7	8	9	10	11	12	13	14	15	16
$y\,(\mathrm{mm})^{(a)}$	5	10	15	20	25	30	35	40	45	50	55	60	65	70	75	80
$r_l\,(\mathrm{mm})^{(b)}$	1.48	1.48	1.47	1.46	1.45	1.44	1.42	1.4	1.37	1.34	1.31	1.28	1.24	1.19	1.14	1.09

[(a)] y: The distance from the center of the cylinder in the l layer that lies along the $+y$-direction to the x-axis.
[(b)] r_l: The radius of the cylinder in the l layer that lies along the $+y$-direction.

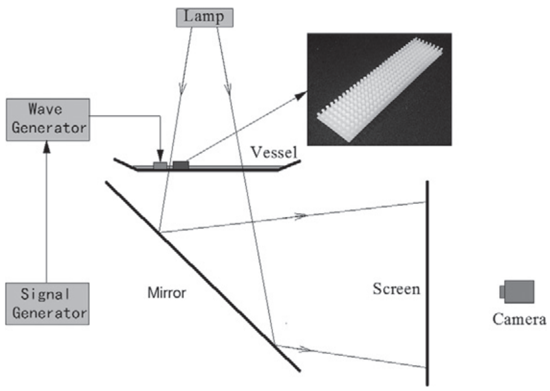

Fig. 2: Diagram of the experimental setup [30]. The inset (top, right) represents the GRIN lens for liquid surface waves.

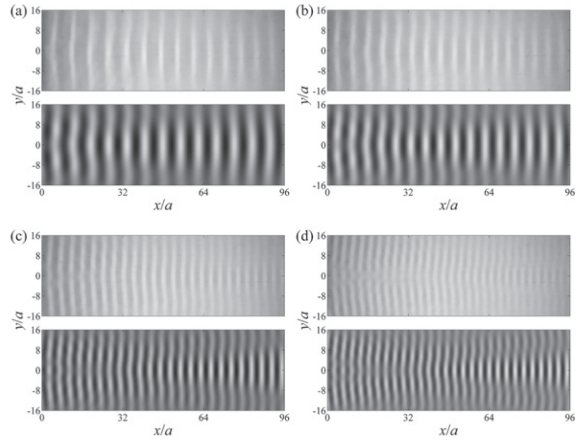

Fig. 3: The spatial distributions of outgoing liquid surface waves at 5.76 (a), 6.72 (b), 8.94 (c), and 10.09 Hz (d). The upper and lower panels represent the observed and simulated wave patterns, respectively. The dark and light areas represent positive and negative vibrations, respectively.

signal generator. The diagram of the experimental setup is illustrated in fig. 2. A detailed description of a similar experimental setup can be found elsewhere [30,34].

Results and discussion. – Figure 3 shows the patterns of liquid surface waves flowing out from the GRIN lens at different frequencies. The observed snapshots in the experiment are displayed in the upper panels. The dark and light areas in these snapshots represent positive and negative vibrations, respectively. We can see that the outgoing waves along the $+x$-direction are curved at all given frequencies. However, the largest amplitudes of liquid surface waves cannot be clearly observed as a result of the uniform background intensity. As a comparison, the simulated wave patterns at the same frequencies have been calculated by using the finite element method and shown in the lower panels in fig. 3. Similar wave patterns can be found in the simulated results. The fact that the lightest and darkest regions of a simulated image correspond to the local extrema or antinodes of the wave patterns indicates that the largest amplitudes of liquid surface waves appear at certain distances from the lens, confirming the fact that the GRIN lens can focus liquid surface waves at certain distances. It is clear from the dispersion relation of liquid surface waves that the corresponding wavelengths of the given frequencies of 5.76, 6.72, 8.94, and 10.09 Hz are $7a$, $5.8a$, $4a$, and $3.4a$, respectively. Although the $\lambda = 3.4a$ is not in the long-wavelength limit, the focusing effect is also realized owing to the fact that the gradual refractive index profile still exists in the lens structure. Nevertheless, wave focusing is no longer available for a shorter wavelength because the higher frequencies fall in the band gap.

In order to show the focusing effects clearly and to analyze the discrepancies in the results of the experiment, the spatial intensity of liquid surface waves need to be derived from both the experiment and the simulation. Figure 4(a) shows that the simulated spatial distribution of the emitted-wave intensity corresponds to fig. 3(c). An obvious focusing effect is displayed. A narrow region along the $+x$-direction showing high intensity can clearly be seen. The wave intensities along the x-axis at $y = 0$ have been plotted in fig. 4(b). A maximum transmitted wave intensity can be found at $x = 70.56a$. Figure 4(c) illustrates the wave intensity along the y-axis at $x = 70.56a$. The full transverse width at half the maximum wave intensity along the y-axis is $3.8a$ and is less than one wavelength.

Assuming that the brightness of the wave patterns can be considered as linearly proportional to the amplitudes of liquid surface waves [34], the spatial intensity from the experiment can be obtained by instantaneously averaging the spatial wave patterns. Although the liquid employed in the experiment has small capillary length and viscosity, the energy loss cannot be overlooked. As we can see in fig. 5, the amplitude changes as a function of

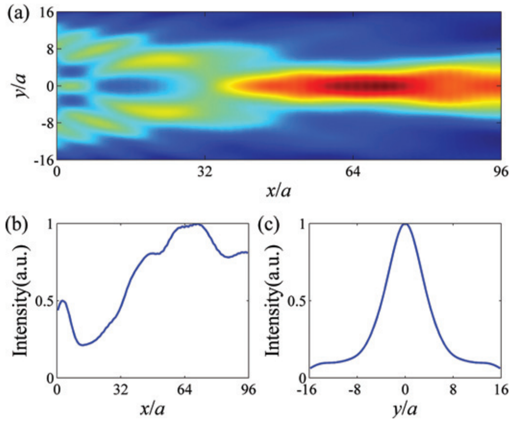

Fig. 4: (Color online) Simulated results for the focusing of a plane liquid surface wave at a frequency of 8.94 Hz. (a) The spatial intensity of the waves in the $+x$-direction. The light region indicates high intensity. (b) Transmitted wave intensity along the x-axis at $y = 0$. (c) Transmitted wave intensity along the y-axis at $x = 70.56a$.

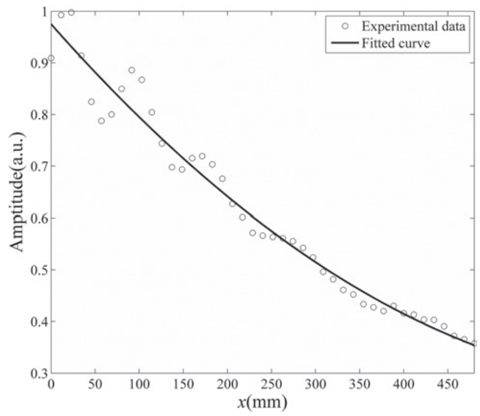

Fig. 5: The wave amplitude change as a function of the travel distance of liquid surface waves at 8.94 Hz.

the distance of plane waves travelling at a the frequency of 8.94 Hz when the waves' journey along the observation region (16 cm × 48 cm) is plotted. Obviously, the wave amplitude decreases significantly when the travelling distance is increased. Only about one-third of the amplitude remains when the waves travel a distance of 48 cm, which differs considerably from the assumption of no energy loss observed in the simulation. Hence, the difference in the distribution of the wave intensity between the experimental and simulated results is to be expected.

To minimize the difference caused by the energy loss in the experiment and to present a better description of the focusing effect, the measured results of the spatial wave intensity at 8.94 Hz in the experiment have been manipulated by a compensation function, which is derived from fig. 5 so as to include the reduction of the wave amplitude as a factor. The processed experimental results of emitted-wave intensity are shown in fig. 6. Figure 6(a) shows a wave focusing effect similar to that plotted in fig. 4(a). The maximum transmitted wave intensity at $x = 56.4a$, *i.e.* the focal point, is clearly illustrated in fig. 6(b), showing the wave intensity along the x-axis at $y = 0$. In addition, the wave intensity along the y-axis at $x = 56.4a$ is illustrated in fig. 6(c). The full transverse width at half the maximum wave intensity along the x-axis is $4.4a$.

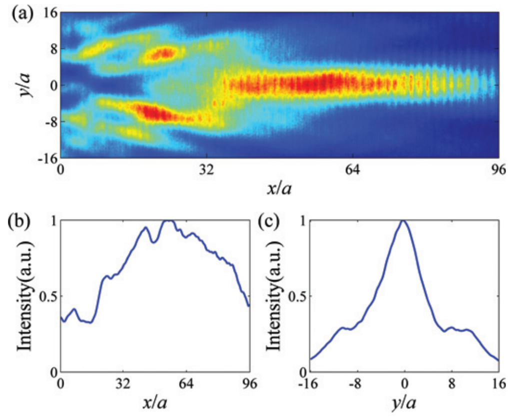

Fig. 6: (Color online) Experimental results for the focusing of a plane liquid surface wave at a frequency of 8.94 Hz. (a) Spatial intensity of the waves in the $+x$-direction. The light region indicates high intensity. (b) Transmitted wave intensity along the x-axis at $y = 0$. (c) Transmitted wave intensity along the y-axis at $x = 56.4a$.

We are aware that a small discrepancy exists in the position of the focal point between the experiment and the simulations. The position of the focal point along the x-axis for the plane wave at a frequency of 8.94 Hz is about $x = 56.4a$ in the results of the experiment, while, in the simulation, it is about $x = 70.56a$. Similar features not only appear at other frequencies that we have observed, but also exist in Yang's study concerning the biconvex lens [34]. As mentioned before and illustrated in Yang's study, the discrepancies seem to be caused by the capillary effect and the viscosity of the liquid used in the experiment. It is these two factors that cause the significant energy loss of the waves when they travel. Meanwhile, due to the limitations of the vessel employed in the experiment, the distance between the two nearest cylinders is not large enough so that the capillary effects will, to a certain extent, influence the effective refractive index profile of the lens. For these reasons, the results of the experiment differ from the theoretical calculations derived under ideal conditions. A better correspondence between experimental and simulated results could be expected if large lattice sizes were used in a larger vessel thereby lessening the capillary effect. It should be noted that in the above discussion, the measured region and focus distance are already comparable to the lattice constant of the lens. In the case of $a = H = 1$ m, for example, the frequency corresponding to the working wavelength of $4a$ is 0.598 Hz, and the ideal position of the focal point is about 70.56 m.

Meanwhile, elongating the long side of the lens, shortening its short side, and decreasing the difference of the refractive indexes inside the lens are all effective methods by which to obtain a further focus distance at a certain lattice constant, liquid depth, and wave frequency.

Conclusions. – In this paper, the focusing properties of a GRIN lens for liquid surface waves have been investigated theoretically and experimentally. The GRIN lens was created simply by using an array of vertical cylinders with gradual variational radii with an effective gradual index profile in the long-wavelength limit. Both the experimental observations and numerical simulations confirm its broadband performance. We have concluded that GRIN lenses are feasible as well as reliable for liquid surface waves, and their focusing ability can be used to concentrate the wave energy so as to enhance the harvest efficiency of water or ocean power. In addition, the design method of the GRIN medium can be potentially applied to the construction of refractive devices for surface wave control in hydraulic and ocean engineering.

* * *

This work was supported by the National Basic Research Program of China (2013CB035901), the National Natural Science Foundation of China (Grant Nos. 51179171, 51279180, and 51079127), and the Science Technology Department of Zhejiang Province (Grant No. 2013C33043).

REFERENCES

[1] Yablonovitch E., *Phys. Rev. Lett.*, **58** (1987) 2059.
[2] John S., *Phys. Rev. Lett.*, **58** (1987) 2486.
[3] Ho K. M., Chan C. T. and Soukoulis C. M., *Phys. Rev. Lett.*, **65** (1990) 3152.
[4] Chan C. T., Ho K. M. and Soukoulis C. M., *Europhys. Lett.*, **16** (1991) 563.
[5] Sigalas M. M. and Economou E. N., *J. Sound Vib.*, **158** (1992) 377.
[6] Kushwaha M. S., Halevi P., Dobrzynski L. and Djafari-Rouhani B., *Phys. Rev. Lett.*, **71** (1993) 2022.
[7] Vasseur J., Deymier P., Chenni B., Djafari-Rouhani B., Dobrzynski L. and Prevost D., *Phys. Rev. Lett.*, **86** (2001) 3012.
[8] Liu Z. Y., Zhang X. X., Yiwei M., Zhu Y. Y., Yang Z. Y., Chan C. T. and Sheng P., *Science*, **289** (2000) 1734.
[9] Luo C. Y., Johnson S. G., Joannopoulos J. D. and Pendry J. B., *Phys. Rev. B*, **65** (2002) 201104(R).
[10] Ambati M., Fang N., Sun C. and Zhang X., *Phys. Rev. Lett.*, **75** (2007) 195447.
[11] Smith D. R., Padilla W. J., Vier D. C., Nemat-Nasser S. C. and Schultz S., *Phys. Rev. Lett.*, **84** (2000) 4184.
[12] Lai Y., Wu Y., Sheng P. and Zhang Z. Q., *Nat. Mater.*, **10** (2011) 620.
[13] Pendry J. B., Schurig D. and Smith D. R., *Science*, **312** (2006) 1780.
[14] Chen H. Y. and Chan C. T., *Appl. Phys. Lett.*, **91** (2007) 183518.
[15] Biswas R., Ozbay E., Temelkuran B., Bayindir M., Sigalas M. M. and Ho K.-M., *J. Opt. Soc. Am. B*, **18** (2001) 1684.
[16] Bulu I., Caglayan H. and Ozbay E., *Appl. Phys. Lett.*, **83** (2003) 3263.
[17] Kwon S.-H., Ryu H.-Y., Kim G.-H., Lee Y.-H. and Kim S.-B., *Appl. Phys. Lett.*, **83** (2003) 3870.
[18] Qiu C. Y., Liu Z. Y., Shi J. and Chan C. T., *Appl. Phys. Lett.*, **86** (2005) 224105.
[19] Qiu C. Y. and Liu Z. Y., *Appl. Phys. Lett.*, **89** (2006) 063106.
[20] Ke M. Z., Liu Z. Y., Pang P., Wang W. G., Cheng Z. G., Shi J., Zhao X. Z. and Wen W. J., *Appl. Phys. Lett.*, **88** (2006) 263505.
[21] Ke M. Z., Liu Z. Y., Pang P., Qiu C. Y., Zhao D. G., Peng S. S., Shi J. and Wen W. J., *Appl. Phys. Lett.*, **90** (2007) 083509.
[22] Mciver P., *J. Fluid Mech.*, **424** (2000) 101.
[23] Torres M., Adrados J., Montero De Espinosa F., García-Pablos D. and Fayos J., *Phys. Rev. E*, **63** (2000) 011204.
[24] Ha Y.-K., Kim J.-E., Park H. Y. and Lee I.-W., *Appl. Phys. Lett.*, **81** (2002) 1341.
[25] Hu X. H., Shen Y. F., Liu X. H., Fu R. T., Zi J., Jiang X. Y. and Feng S. L., *Phys. Rev. E*, **68** (2003) 037301.
[26] Hu X. H., Shen Y. F., Liu X. H., Fu R. T. and Zi J., *Phys. Rev. E*, **68** (2003) 066308.
[27] Chen L.-S., Kuo C.-H., Ye Z. and Sun X., *Phys. Rev. E*, **69** (2004) 066308.
[28] Jeong T. S., Kim J.-E., Park H. Y. and Lee I.-W., *Appl. Phys. Lett.*, **85** (2004) 1645.
[29] Shen Y. F., Liu X. H., Tang Y. F., Chen Y. F. and Zi J., *J. Phys.: Condens. Matter*, **17** (2005) L287.
[30] Hu X. H., Shen Y. F., Liu X. H., Fu R. T. and Zi J., *Phys. Rev. E*, **69** (2004) 030201(R).
[31] Farhat M., Guenneau S., Enoch S., Tayeb G., Movchan A. B. and Movchan N. V., *Phys. Rev. E*, **77** (2008) 046308.
[32] Farhat M., Guenneau S., Enoch S. and Movchan A., *J. Comput. Appl. Math.*, **234** (2010) 2011.
[33] Hu X. H. and Chan C. T., *Phys. Rev. Lett.*, **95** (2005) 154501.
[34] Yang J., Tang Y. F., Ouyang C. F., Liu X. H., Hu X. H. and Zi J., *Appl. Phys. Lett.*, **95** (2009) 094106.
[35] Shen Y. F., Chen K. X., Chen Y. F., Liu X. H. and Zi J., *Phys. Rev. E*, **71** (2005) 036301.
[36] Hu X. H., Chan C., Ho K.-M. and Zi J., *Phys. Rev. Lett.*, **106** (2011) 174501.
[37] Hu X. H., Yang J., Zi J., Chan C. T. and Ho K.-M., *Sci. Rep.*, **3** (2013) 1916.
[38] Mei J., Qiu C. Y., Shi J. and Liu Z. Y., *Phys. Lett. A*, **373** (2009) 2948.
[39] Mei J., Qiu C. Y., Shi J. and Liu Z. Y., *Wave Motion*, **47** (2010) 131.
[40] Wang Z. Y., Zhang P., Zhang Y. Q. and Nie X. F., *Physica B*, **431** (2013) 75.
[41] Farhat M., Enoch S., Guenneau S. and Movchan A. B., *Phys. Rev. Lett.*, **101** (2008) 134501.

[42] Chen H. Y., Yang J., Zi J. and Chan C. T., *EPL*, **85** (2009) 24004.

[43] Torrent D. and Sánchez-Dehesa J., *New J. Phys.*, **10** (2008) 023004.

[44] Gomez-Reino C., Perez M. V. and Bao C., *Gradient-Index Optics-Fundamentals and Applications* (Springer-Verlag, Berlin, Heidelberg, New York) 2002.

[45] Kurt H. and Citrin D. S., *Opt. Express*, **15** (2007) 1240.

[46] Juluri B. K., Lin S.-C. S., Walker T. R., Jensen L. and Huang T. J., *Opt. Express*, **17** (2009) 2997.

[47] Lin S.-C. S., Huang T. J., Sun J.-H. and Wu T.-T., *Phys. Rev. B*, **79** (2009) 094302.

[48] Climente A., Torrent D. and Sánchez-Dehesa J., *Appl. Phys. Lett.*, **97** (2010) 104103.